

Large deviations induced entanglement transitions

Udaysinh T. Bhosale*

Indian Institute of Science Education and Research, Dr. Homi Bhabha Road, Pune 411 008, India.

(Dated: December 14, 2024)

The probability of large deviations of the smallest Schmidt eigenvalues for random pure states of bipartite systems, denoted as A and B , is computed analytically using a Coulomb gas method. It is shown that this probability, for large N , goes as $\exp[-\beta N^2 \Phi(\zeta)]$, where the parameter β is the Dyson index of the ensemble, ζ is the large deviation parameter while the rate function $\Phi(\zeta)$ is calculated exactly. Equilibrium Coulomb charge density is derived for the large deviations of the extreme (largest and smallest) Schmidt eigenvalues. Effect of these deviations is studied on the bipartite entanglement measured using the von Neumann entropy. Effect of these deviations is also studied on the entanglement between subsystems 1 and 2, obtained by further partitioning the subsystem A , using the properties of the density matrix's partial transpose ρ_{12}^T . The density of states of ρ_{12}^T is found to be close to the semicircle law. The entanglement properties are captured very well by a simple random matrix model for the partial transpose. The model predicts the entanglement transition across a critical large deviation parameter ζ . Log negativity is used to quantify the entanglement between subsystems 1 and 2. Analytical formulas for it are derived using the simple model. Numerical simulations are in excellent agreement with the analytical results.

PACS numbers: 05.45.Mt, 03.65.Ud, 03.67.-a

I. INTRODUCTION

The large deviation is defined as the atypical behavior of a system from its average state. Its theory is an active field of research in probability and statistics [1]. This theory has found applications in the field of random matrices [2–6], quantum entanglement [7–12], economics [13], geophysics, hydrology [14], image processing [15, 16] etc. This theory is tested in the context of coupled lasers and found to agree very well with the experiment [17]. This theory has been successfully applied in the field of quantum information to study entanglement. Entanglement is a central property of quantum mechanics which is not there in classical physics. In fact recently it is shown that any theory which has a classical limit must have entanglement as an inevitable feature [18]. It is studied extensively since it is a critical resource for the quantum computation and information tasks [19], quantum teleportation [20], dense coding [21], etc. Entanglement has been studied in various experiments using optics, superconductivity, etc [19]. Recently it is shown theoretically that the charging power of quantum batteries can be enhanced using entanglement [22]. In this paper, we are interested in the applications of the large deviation theory to study the entanglement transitions.

Let us start by considering a standard bipartite system $A \otimes B$ which is composed of two smaller subsystems A and B having Hilbert spaces $\mathcal{H}_A^{(N)}$ and $\mathcal{H}_B^{(M)}$ having dimensions N and M respectively. Whereas the full system is described by the product Hilbert space $\mathcal{H}_{AB}^{(MN)} = \mathcal{H}_A^{(N)} \otimes \mathcal{H}_B^{(M)}$. Here, the simple case of $N = M$ is studied in detail but the results can be extended to the $N \neq M$ case. Consider $|\psi\rangle = \sum_{i=1}^N \sum_{\alpha=1}^M c_{i,\alpha} |i\rangle \otimes |\alpha\rangle$ a

normalized pure state of the full system A and B , where $|i\rangle \otimes |\alpha\rangle$ is the orthonormal basis of \mathcal{H}_{AB} . The density matrix is given as $\rho = |\psi\rangle\langle\psi|$ which satisfies $\text{Tr}[\rho]=1$ condition. The reduced density matrix of the subsystem A is given by $\rho_A = \text{Tr}_B[\rho] = \sum_{\alpha=1}^M \langle \alpha | \rho | \alpha \rangle$. Similarly, the subsystem B is described by $\rho_B = \text{Tr}_A[\rho]$. Using the singular value decomposition of the matrix $c_{i,\alpha}$ one obtains the Schmidt decomposition form:

$$|\psi\rangle = \sum_{i=1}^N \sqrt{\lambda_i} |u_i^A\rangle \otimes |v_i^B\rangle \quad (1)$$

where $|u_i^A\rangle$ and $|v_i^B\rangle$ are the eigenvectors of ρ_A and ρ_B respectively, with the same eigenvalue λ_i . The $\lambda_i \in [0, 1]$ for all $i = 1$ to N such that $\sum_{i=1}^N \lambda_i = 1$.

Given the Schmidt eigenvalues $\{\lambda_i\}$ ($i = 1 \dots N$) the entanglement between A and B , measured using von Neumann entropy, is given by

$$S_{VN} = -\text{tr}(\rho_A \log \rho_A) = -\sum_{i=1}^N \lambda_i \ln(\lambda_i). \quad (2)$$

It is a good measure of entanglement for a bipartite pure state [23, 24]. Study of the two extreme eigenvalues, the largest $\lambda_{\max} = \max(\lambda_1, \lambda_2, \dots, \lambda_N)$ and the smallest $\lambda_{\min} = \min(\lambda_1, \lambda_2, \dots, \lambda_N)$, is important as they give useful information about the nature of entanglement between the subsystems A and B [7, 9, 10, 25–29]. It can be seen easily that the conditions $\sum_{i=1}^N \lambda_i = 1$ and $\lambda_i \in [0, 1]$ for $i = 1 \dots N$ imply $0 \leq \lambda_{\min} \leq 1/N$ and $1/N \leq \lambda_{\max} \leq 1$.

To understand the importance of the extreme eigenvalues, let us first consider the following limiting situations of the largest eigenvalue. Suppose that λ_{\max} takes the maximum allowed value 1. Then due to the normalization constraints $\sum_{i=1}^N \lambda_i = 1$ and $\lambda_i \in [0, 1]$ for all i ,

* udaybhosale0786@gmail.com

it follows that all the rest ($N - 1$) eigenvalues must be identically equals to 0. Thus, using Eq. (1) for this case implies that the state $|\psi\rangle$ is fully *unentangled*. On the other hand, if λ_{\max} takes its lowest allowed value $1/N$ then the constraint $\sum_{i=1}^N \lambda_i = 1$ implies that $\lambda_i = 1/N$ for all i . In this case, it can be shown that the state $|\psi\rangle$ is *maximally* entangled as it maximizes the von Neumann entropy $S_{VN} = \ln(N)$.

Now, consider the limiting situations of the minimum eigenvalue. Suppose, λ_{\min} takes the maximum allowed value $1/N$. Then, the constraint $\sum_{i=1}^N \lambda_i = 1$ implies that $\lambda_i = 1/N$ for all i . Thus, the state $|\psi\rangle$ is *maximally* entangled. When λ_{\min} takes the minimum allowed value 0 then not much information on the entanglement in the state $|\psi\rangle$ is obtained. But, using the Schmidt decomposition one can see that the dimension of the effective Hilbert space of the subsystem A is now reduced from N to $N - 1$. This also implies that the maximum von Neumann entropy it can take is reduced from $\ln(N)$ to $\ln(N - 1)$.

The pure state $|\psi\rangle$ is called random when it is sampled uniformly from the unique Haar measure that is invariant under unitary transformations. As a result, the eigenvalues $\{\lambda_i\}$'s also become random variables. In that case, the distributions of the extreme eigenvalues of ρ_A have been studied in detail for various cases of N and M [7, 9, 10, 25–29]. The distribution of the minimum eigenvalue for $\beta = 1, 2$ and finite $N = M$ was derived in [9, 26] while $N \neq M$ case is addressed in [28]. Here, β is the Dyson index and it takes values 1, 2 and 4 for real, complex and symplectic case respectively. Similarly, the maximum eigenvalue distribution for large $N = M$ and all β 's is given in [7, 10], which include the small and large deviation laws. In fact, the distribution of all the Schmidt eigenvalues for large N and M is known as the Marcenko-Pastur function [10, 30] (see Eq. (4)). Probability distribution of the Renyi entropies, a measure of entanglement, for a random pure state of a large bipartite quantum system has been derived analytically [7, 10, 31].

If the constraint of eigenvalues summing to one is removed and $c_{i,\alpha}$ are independent and identically distributed (i.i.d.) random variables, real or complex, drawn from a Gaussian distribution, then ρ_A belongs to the Wishart ensemble. These matrices have found applications in the fields like finance [32], nuclear physics [33, 34], quantum chromodynamics [35, 36], knowledge networks [37], etc. For this ensemble it is shown that the probability distribution of the *typical and small* fluctuations of the extreme eigenvalues is given by Tracy-Widom distribution [38–40], while the *atypical and large* fluctuations obey a different distribution having limiting form of the Tracy-Widom in the limit of small fluctuations [2, 6].

Turning our attention to the ρ_A , whose eigenvalues sum to one, the large deviation function for the maximum eigenvalue is derived in [10] using the Coulomb gas method. To be specific, the probability distribution function $P(N\lambda_{\max} = a)$ where $a > 1$ is derived. It is also shown that its typical fluctuations around the average

$4/N$ follow the Tracy-Widom Distribution. Explicit expression for the equilibrium charge density is not given in [10]. In this paper, the equilibrium charge density when $N\lambda_{\max} \leq a$ is derived for $1 < a < 4$. Similarly, the large deviation function for the minimum eigenvalue and the associated equilibrium charge density is derived. Thus, a generalized Macenko-Pastur function is derived when there are large deviations either in minimum or maximum eigenvalue. For these derivations, the Coulomb gas technique from the random matrix theory is used. The same technique has been used successfully earlier in the field of random matrices [2–4, 7, 10, 31, 40–46].

The structure of the paper is as follows: In Sec. II some known and the relevant results of the reduced density matrix are presented. In Sec. III (Sec. IV) the large deviation function for the maximum (minimum) eigenvalue and the associated equilibrium density of states of the reduced density matrix is derived. For these derivations the Coulomb gas method from the random matrix theory is used. In Sec. V the effect of large deviations of the extreme eigenvalues on the entanglement between the subsystems A and B is studied in detail. Then, the subsystem A is divided into two equal parts 1 and 2 of dimension N_1 each such that $N = N_1^2$. In Sec. VI the effect of these large deviations are studied on the entanglement between subsystems 1 and 2.

II. STATISTICAL PROPERTIES OF THE REDUCED DENSITY MATRIX

Consider the state $|\psi\rangle$ of the quantum system of A and B is drawn from the ensemble of random pure states. The joint probability density function (jpdf) of the eigenvalues of the reduced density matrix ρ_A is then given as follows [47, 48]:

$$P[\{\lambda_i\}] = K_{M,N} \delta\left(\sum_{i=1}^N \lambda_i - 1\right) \prod_{i=1}^N \lambda_i^{\frac{\beta}{2}(M-N+1)-1} \times \prod_{i < j} |\lambda_i - \lambda_j|^\beta, \quad (3)$$

For the $N = M$ case the jpdf corresponds to Hilbert-Schmidt measure whose statistical properties are well studied [49]. The normalization constant $K_{M,N}$ is calculated using the Selberg's integral [48]. For large N and M , the density of the eigenvalues is given by an appropriately scaled Marcenko-Pastur (MP) function [10, 30],

$$f(\lambda) = \frac{NQ}{2\pi} \frac{\sqrt{(\lambda_+ - \lambda)(\lambda - \lambda_-)}}{\lambda} \quad (4) \\ \lambda_\pm = \frac{1}{N} \left(1 + \frac{1}{Q} \pm \frac{2}{\sqrt{Q}} \right),$$

where $\lambda \in [\lambda_-, \lambda_+]$, $Q = M/N$ and $Nf(\lambda)d\lambda$ is the number of eigenvalues in the range λ to $\lambda + d\lambda$. For $Q = 1$ ($N = M$) the distribution has a divergence at the origin

and it vanishes at $4/N$. Whereas for $Q > 1$ the eigenvalues are bounded away from zero.

The purity of the subsystem, defined as $\text{tr}[(\rho_A)^2]$, lies between $1/N$ and 1. For the minimum value, ρ_A is maximally mixed and is equal to I/N while for the maximum value the two subsystems are unentangled. The average purity of the subsystem A for the random state $|\psi\rangle$ is given by

$$\langle \text{tr}[(\rho_A)^2] \rangle = \frac{N+M}{NM+1} \approx \frac{1}{N} + \frac{1}{M}, \quad (5)$$

where the last approximation is valid for $N, M \gg 1$ [50]. An exact formula for the average of the von Neumann entropy is evaluated over the probability density in Eq. (3). It is given as follows [51–53]:

$$\begin{aligned} \langle S_{VN} \rangle &= \sum_{m=M+1}^{NM} \frac{1}{m} - \frac{N-1}{2M} \\ &\approx \log(N) - \frac{N}{2M} \quad \text{for } 1 \ll N \leq M. \end{aligned} \quad (6)$$

This implies that, practically there is very little information about the full pure state in a subsystem. More precisely, in a random pure state there is less than one-half unit of information on an average in the smaller subsystem of the total system.

III. LARGE DEVIATION FUNCTION FOR THE MINIMUM EIGENVALUE

In this case all the rescaled eigenvalues $N\lambda$ are constrained to lie on the right side of a wall at ζ . This condition is satisfied when $N\lambda_{\min} \geq \zeta$. Since, λ_{\min} satisfies the condition $0 \leq N\lambda_{\min} \leq 1$ this implies $0 \leq \zeta \leq 1$. First, the results for this case will be summarized which then will be proved in Sec. III A. In this case the density of states of the rescaled eigenvalues for large N is found as follows:

$$\rho(\lambda') = \frac{1}{2\pi(1-\zeta)} \sqrt{\frac{4-3\zeta-\lambda'}{\lambda'-\zeta}}, \quad \zeta \leq \lambda' \leq 4-3\zeta, \quad (7)$$

where $\lambda' = N\lambda$ and $0 \leq \zeta \leq 1$. It has a divergence at ζ and vanishes at $4-3\zeta$. An example for this case is demonstrated in Fig. 1 for the case of $\zeta = 0.5$. For this case one obtains the following distribution:

$$\rho(\lambda') = \frac{1}{\pi} \sqrt{\frac{5-2\lambda'}{2\lambda'-1}}, \quad \frac{1}{2} \leq \lambda' \leq \frac{5}{2}. \quad (8)$$

In the same figure the Monte Carlo simulations of $N = 100$ is shown. It shows a good agreement between the formula and the numerical simulations.

A. Evaluation of the density of states in Eq. (7) using the Coulomb gas method

The mapping of the eigenvalues of a random matrix to a Coulomb gas problem is a well established method in

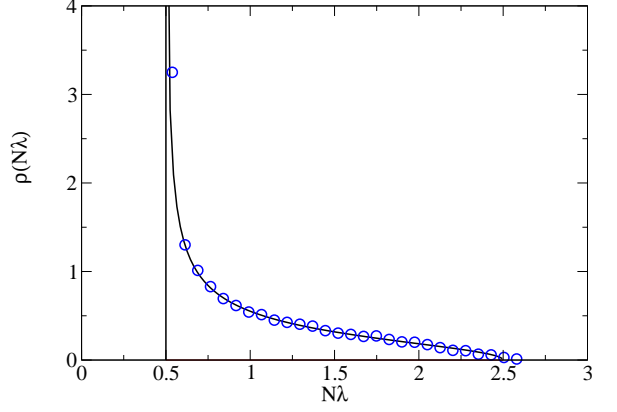


FIG. 1. (Color online) Equilibrium density of the Coulomb fluid (Eq. (8)) when all the charges are constrained to the right of $\zeta = 0.5$ (black solid line) together with the Monte Carlo simulations (blue circles) for the case $N = M = 100$.

random matrix theory [54]. This method has been used in variety of problems which include finding the distribution of the extreme eigenvalues of the Gaussian and wishart matrices [2–4, 6, 40], quantum transport in chaotic cavities [55, 56], the index distribution for the Gaussian random fields [57] and the Gaussian ensemble [58, 59]. The unit trace constraint $\sum_{i=1}^N \lambda_i = 1$ implies that the typical amplitude of the eigenvalues is $\lambda_{typ} \sim 1/N$. Whereas in the case of the Wishart ensemble $\lambda_{typ}^W \sim N$. This implies that the scaling with N , for large N , differs in both the cases. But it should be noted that the effect of the trace constraint does not imply the rescaling of the Wishart results by a factor of $1/N^2$. This effect of the trace constraint leads to a different and new behavior which includes a condensation transition, which is absent in the Wishart ensembles [7, 10, 31]. In this paper too the effect of this trace constraint will be observed on the density of states for the large deviations of the extreme eigenvalues.

This density of states in Eq. (7) corresponds to the following probability:

$$\begin{aligned} P(N\lambda_{\min} > \zeta) &= P(N\lambda_1 > \zeta, N\lambda_2 > \zeta, \dots, N\lambda_N > \zeta) \\ &= \frac{\int_{\zeta}^{\infty} \dots \int_{\zeta}^{\infty} P[\{\lambda_i\}] \prod_{i=1}^N d\lambda_i}{\int_0^{\infty} \dots \int_0^{\infty} P[\{\lambda_i\}] \prod_{i=1}^N d\lambda_i}, \end{aligned} \quad (9)$$

when all the eigenvalues are constrained to be larger than a fixed constant ζ . The joint pdf of the eigenvalues $P[\{\lambda_i\}]$ given in Eq. (3) can be seen as a Boltzmann weight at inverse temperature β :

$$P[\{\lambda_i\}] \propto \exp\{-\beta E[\{\lambda_i\}]\}, \quad (10)$$

where the energy $E[\{\lambda_i\}] = -\gamma \sum_{i=1}^N \ln \lambda_i - \sum_{i < j} \ln |\lambda_i - \lambda_j|$ and $\gamma = \beta/2 - 1$ (for $N = M$ case). This energy is the effective energy of a 2D Coulomb gas of charges where the charges repel each other electrostatically via

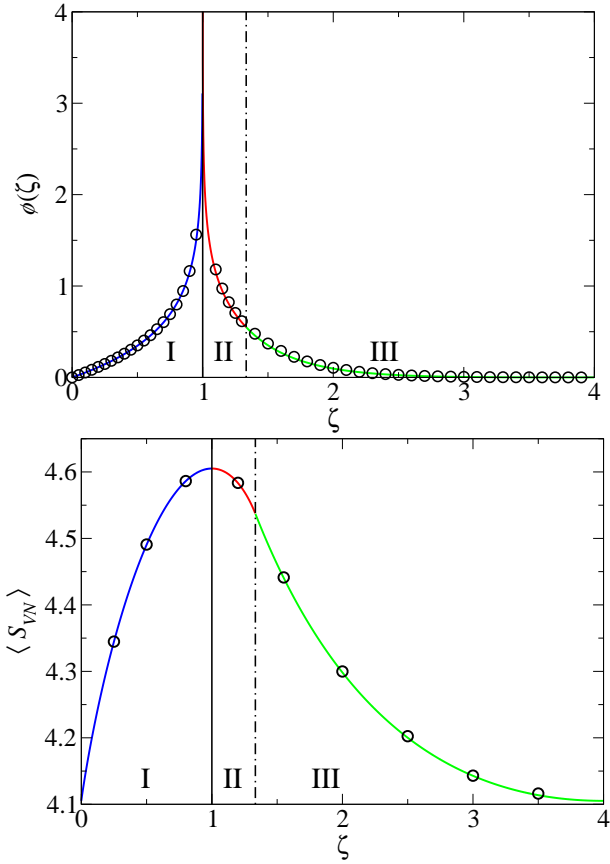


FIG. 2. (Color online) Rate functions (top) and the average von Neumann entropy (bottom) as a function of the barrier position. Region I corresponds to $0 \leq \zeta \leq 1$ when all the charges are on the right side of the barrier. Regions II and III corresponds to $1 \leq \zeta \leq 4/3$ and $4/3 \leq \zeta \leq 4$ respectively when all the charges are on the left side of the barrier. Monte Carlo simulations are shown in both the figures using black circles for $M = N = 100$.

logarithmic interaction in 2D. For large N , the presence of the logarithmic interaction potential term results in the effective energy to be of the order $E \sim O(N^2)$. Thus, to compute the multiple integral in Eq. (9) the method of steepest descent is used. In this method, for large N , the configuration of $\{\lambda_i\}$ which dominates the integral is the one that minimizes the effective energy. For large N , it can be expected that the eigenvalues are close to each other. In that case the saddle point will be highly peaked, i.e. the most probable value and the mean will coincide. Thus, labeling the λ_i by a continuous average density of states $\rho(\lambda, N) = N^{-1} \sum_i \langle \delta(\lambda - \lambda_i) \rangle = N \rho(x)$ where

$$\rho(x) = N^{-1} \sum_i \langle \delta(x - \lambda_i N) \rangle \quad (11)$$

and $x = \lambda N$. Thus, with this the probability of $N \lambda_{\min}$

greater than ζ can be written as

$$P(N \lambda_{\min} > \zeta) \propto \int \mathcal{D}[\rho] \exp \{-\beta N^2 E_\zeta[\rho]\}, \quad (12)$$

where the effective energy $E_\zeta[\rho]$ is given by

$$E_\zeta[\rho] = -\frac{1}{2} \int_\zeta^\infty \int_\zeta^\infty dx dx' \rho(x) \rho(x') \ln |x - x'| + \mu_0 \left(\int_\zeta^\infty dx \rho(x) - 1 \right) + \mu_1 \left(\int_\zeta^\infty dx x \rho(x) - 1 \right) \quad (13)$$

The Lagrange multipliers μ_0 and μ_1 enforce the constraints $\int \rho(x) dx = 1$ (the normalization of the density) and $\sum_i \lambda_i = 1$ (the unit trace) respectively. For large N , the method of steepest descent gives the following:

$$P(N \lambda_{\min} > \zeta) \propto \exp \{-\beta N^2 E_\zeta[\rho_\zeta]\}, \quad (14)$$

where ρ_ζ minimizes the energy (the saddle point):

$$\frac{\delta E_\zeta}{\delta \rho} \Big|_{\rho=\rho_\zeta} = 0. \quad (15)$$

The saddle point equation gives:

$$\int_0^\infty dx' \rho_\zeta(x') \ln |x - x'| = \mu_0 + \mu_1 x. \quad (16)$$

Differentiating with respect to x gives:

$$\mathcal{P} \int_0^\infty dx' \frac{\rho_\zeta(x')}{x - x'} = \mu_1, \quad (17)$$

where \mathcal{P} denotes the Cauchy principal value.

This singular integral equation can be solved by using the Tricomi's theorem [60] which states that if the solution ρ^* has the finite support $[L_1, L_2]$, then the finite Hilbert transform which is defined by the following equation

$$F(x) = \mathcal{P} \int_{L_1}^{L_2} dx' \frac{\rho^*(x')}{x - x'} \quad (18)$$

can be inverted as

$$\rho^*(x) = \frac{-1}{\pi^2 \sqrt{x - L_1} \sqrt{L_2 - x}} \left[C + \mathcal{P} \int_{L_1}^{L_2} dx' \frac{\sqrt{x' - L_1} \sqrt{L_2 - x'}}{x - x'} F(x') \right], \quad (19)$$

where $C = -\pi \int_{L_1}^{L_2} dx \rho^*(x)$. Here, $L_1 = \zeta$ and $F(x) = \mu_1$. The integral in Eq. (19) can be evaluated explicitly to obtain:

$$\rho^*(x) = \frac{1}{\pi \sqrt{x - \zeta} \sqrt{L_2 - x}} \left[1 + \frac{(2(\zeta + L_2) - 4)(\zeta + L_2 - 2x)}{(\zeta - L_2)^2} \right], \quad (20)$$

where $\zeta \leq x \leq L_2$.

Here, the normalization condition $\int_{\zeta}^{L_2} dx \rho^*(x) = 1$ is used to set the constant $C = -\pi$. Whereas $\mu_1 = 4(\zeta + L_2 - 2)/(\zeta - L_2)^2$ is obtained using the constraint $\int_{\zeta}^{L_2} dx x \rho^*(x) = 1$. There is one more unknown L_2 which needs to be fixed. At the two end points ζ and L_2 , the solution $\rho^*(x)$ either vanishes or has an inverse square root divergence (which is integrable). When there is no constraint the density has an inverse square root divergence at the origin and it vanishes at 4. But when the minimum eigenvalue has to satisfy the constraint of being greater than ζ then intuitively it seems that the new density must have same nature at the boundary points as that of when there is no constraint. This is verified numerically for various values of ζ between zero and one. One such illustration is shown in Fig. 1. The condition $\rho(L_2) = 0$ gives $L_2 = 4 - 3\zeta$. Thus, the final density as a function of ζ is given as follows:

$$\rho(x) = \frac{1}{2\pi(1-\zeta)} \sqrt{\frac{4-3\zeta-x}{x-\zeta}}, \quad \zeta \leq x \leq 4-3\zeta. \quad (21)$$

Using $L_2 = 4 - 3\zeta$ the constant μ_1 simplifies to $1/(2(1-\zeta))$. The constant μ_0 is found using Eq. (16) and putting $x = \zeta$. This gives $\mu_0 = \ln(1-\zeta) + (3\zeta-2)/(2(1-\zeta))$. Finally, the saddle point energy is calculated. First the saddle point Eq. (16) is multiplied by $\rho(x)$ then the integration is carried out. Then using Eq. (13) one obtains

$$E_{\zeta}[\rho_{\zeta}] = 3/4 - \ln(1-\zeta)/2. \quad (22)$$

Now, the rate function for the large fluctuations will be calculated. It is defined as follows. For large N the probability $P(N\lambda_{\min} > \zeta) \approx \exp\{-\beta N^2 \Phi(\zeta)\}$ where $\Phi(\zeta)$ is the rate function. The normalized probability is given as follows:

$$P(N\lambda_{\min} > \zeta) \approx \frac{\int \mathcal{D}[\rho] \exp\{-\beta N^2 E_{\zeta}[\rho]\}}{\int \mathcal{D}[\rho] \exp\{-\beta N^2 E[\rho]\}}, \quad (23)$$

where $E_{\zeta}[\rho]$ is given in Eq. (22) and $E[\rho]$ is the effective energy associated to the joint distribution of the eigenvalues without any constraint i.e. $\zeta = 0$ in Eq. (22). Using the steepest descent method for both the numerator and the denominator one obtains the following:

$$\begin{aligned} P(N\lambda_{\min} > \zeta) &\approx \frac{\exp\{-\beta N^2 E_{\zeta}[\rho_{\zeta}]\}}{\exp\{-\beta N^2 E[\rho^*]\}} \\ &\approx \exp\{-\beta N^2 \Phi(\zeta)\}, \end{aligned} \quad (24)$$

with $\Phi(\zeta) = E_{\zeta}[\rho_{\zeta}] - E[\rho^*]$ and where ρ^* (resp. ρ_{ζ}) is the density that minimizes the energy $E[\rho]$ (resp. $E_{\zeta}[\rho]$). The density $\rho^*(x)$ is thus simply the rescaled average density of states given in Eq. (4) (for $Q = 1$) which corresponds to $\zeta = 0$ case in Eq. (22). Finally, the rate function is given as follows:

$$\Phi(\zeta)_I = E_{\zeta}[\rho_{\zeta}] - E[\rho^*]_{\zeta=0} = -\frac{\ln(1-\zeta)}{2} \quad (25)$$

and is plotted in Fig. 2 (region **I** of top figure). It shows a divergence as $\zeta \rightarrow 1^-$. Whereas it vanishes at $\zeta = 0$ which is consistent with the no constraint condition. It is compared with the same obtained using Monte Carlo simulations and both of them agrees with each other very well. The large deviations for the minimum eigenvalue of the Wishart ensemble (where there is no trace constraint) is studied earlier in Ref.[6]. Our results, namely the rate function and the density of states differ from that of Ref.[6]. This can be attributed to the trace constraint on the reduced density matrices.

IV. LARGE DEVIATION FUNCTION FOR THE MAXIMUM EIGENVALUE

In this section, the question addressing the constraint on all the eigenvalues being less than a fixed constant ζ is studied. This is equivalent to the condition that $\lambda_{\max} \leq \zeta$. For equal dimensionality $N = M$ case i.e. $Q = 1$ the rescaled eigenvalues lie in the interval $(0, 4]$ (refer Eq. (4)). The barrier position ζ is effective only when $\zeta \leq 4$. Taking into consideration that the sum of the eigenvalues is one implies $1/N \leq \lambda_{\max} \leq 1$. Thus, we get the following:

$$1 \leq \zeta \leq 4. \quad (26)$$

Throughout this paper, whenever ζ lies between zero (one) and one (four) it refers to the fact $N\lambda_{\min} \geq \zeta$ ($N\lambda_{\max} \leq \zeta$).

In this case the numerical simulations using the Monte Carlo method are performed. It is found that there are two regions depending on the nature of the density which shows a transition at $\zeta = 4/3$. Thus, there are two sub cases. Case one ($4/3 \leq \zeta \leq 4$): the density has a support on $[0, \zeta]$ and has a divergence at both the boundaries. Case two ($1 \leq \zeta \leq 4/3$): the density has a support on $[L_1(\zeta), \zeta]$. In this case it vanishes at $L_1(\zeta)$ and has a divergence at ζ . The analytical results for both these cases will be summarized. These results and the existence of the transition point $\zeta = 4/3$ will be derived analytically in Secs. IV A and IV B.

Case one:

$$\frac{4}{3} \leq \zeta \leq 4. \quad (27)$$

In this case the density of states is given as follows:

$$\rho(x) = \frac{2\zeta^2 + 4(\zeta-2)(\zeta-2x)}{2\pi\zeta^2\sqrt{x(\zeta-x)}}, \quad 0 \leq x \leq \zeta. \quad (28)$$

The density has a divergence at $x = 0$ and $x = \zeta$.

Case two:

$$1 \leq \zeta \leq \frac{4}{3}. \quad (29)$$

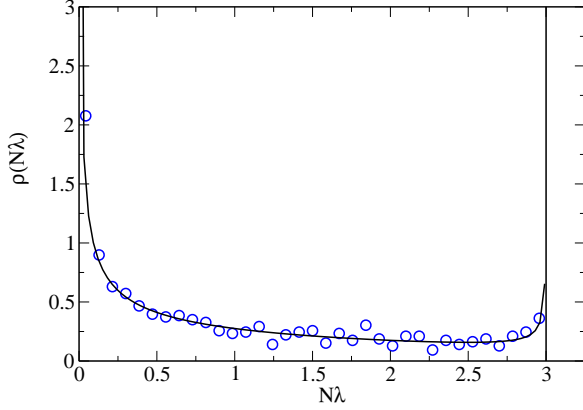


FIG. 3. (Color online) Equilibrium density of the Coulomb fluid, Eq. (31) when all the charges are constrained to the left of $\zeta = 3$ (black solid line) together with the Monte Carlo simulations (blue circles) for the case $N = M = 100$.

In this case the density of states is given as follows:

$$\rho(x) = \frac{1}{2\pi(\zeta-1)} \sqrt{\frac{3\zeta-4+x}{\zeta-x}}, \quad (30)$$

where $4-3\zeta \leq x \leq \zeta$.

It has a divergence at $x = \zeta$ and vanishes at $x = 4 - 3\zeta$. Consider the special case $\zeta = 3$ which fall in the case one category, the analytical distribution is given as follows:

$$\rho(x) = \frac{15-4x}{9\pi\sqrt{x(3-x)}}, \quad 0 \leq x \leq 3. \quad (31)$$

This distribution is plotted in Fig. 3. Similarly, the critical case $\zeta = 4/3$ and $\zeta = 1.2$ are plotted using Eqs. (28) and (30) in Figs. 4 and 5 respectively. Along with the distribution the Monte Carlo simulations of $N = M = 100$ are plotted. It shows a good agreement between the formula and the numerical simulations.

A. The $\frac{4}{3} \leq \zeta \leq 4$ case

The density of states in Eq. (28) corresponds to the following probability:

$$\begin{aligned} P(N\lambda_{\max} < \zeta) &= P(N\lambda_1 < \zeta, N\lambda_2 < \zeta, \dots, N\lambda_N < \zeta) \\ &= \frac{\int_0^\zeta \dots \int_0^\zeta P[\{\lambda_i\}] \prod_{i=1}^N d\lambda_i}{\int_0^\infty \dots \int_0^\infty P[\{\lambda_i\}] \prod_{i=1}^N d\lambda_i}, \end{aligned} \quad (32)$$

when all the eigenvalues are constrained to be smaller than the fixed constant ζ . The lower limit 0 on the integral in the numerator is chosen based on the numerical simulations for the range of ζ considered in this subsection. Following the similar procedure as used in Sec. III A

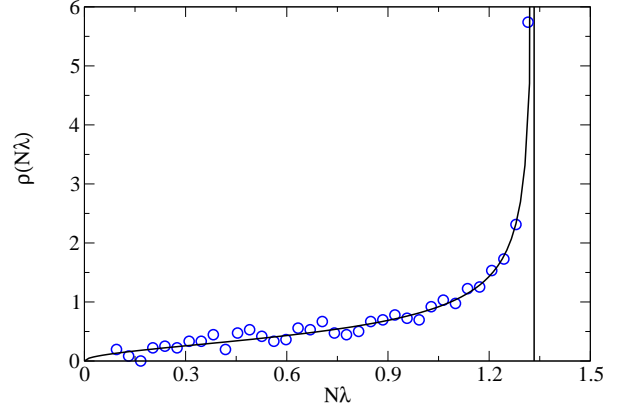


FIG. 4. (Color online) Equilibrium density of the Coulomb fluid, Eq. (28) when all the charges are constrained to the left of the critical point $\zeta = 4/3$ (black solid line) together with the Monte Carlo simulations (blue circles) for the case $N = M = 100$.

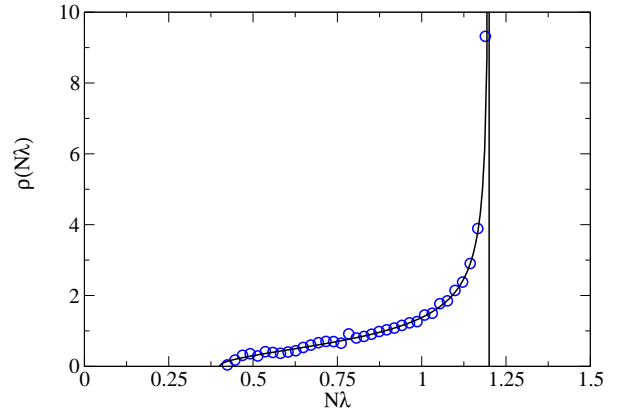


FIG. 5. (Color online) Equilibrium density of the Coulomb fluid, Eq. (28) when all the charges are constrained to the left of $\zeta = 1.2$ (black solid line) together with the Monte Carlo simulations (blue circles) for the case $N = M = 100$.

the effective energy $E_\zeta [\rho]$ is given by

$$\begin{aligned} E_\zeta [\rho] &= -\frac{1}{2} \int_0^\zeta \int_0^\zeta dx dx' \rho(x) \rho(x') \ln |x - x'| \\ &+ \mu_0 \left(\int_0^\zeta dx \rho(x) - 1 \right) + \mu_1 \left(\int_0^\zeta dx x \rho(x) - 1 \right) \end{aligned} \quad (33)$$

where μ_0 and μ_1 are the Lagrange multipliers enforcing the normalization of the density and the unit trace constraint respectively. For the case of large N , the method of steepest descent gives the following:

$$P(N\lambda_{\max} < \zeta) \propto \exp \{ -\beta N^2 E_\zeta [\rho_\zeta] \}, \quad (34)$$

where ρ_ζ minimizes the energy (the saddle point):

$$\left. \frac{\delta E_\zeta}{\delta \rho} \right|_{\rho=\rho_\zeta} = 0. \quad (35)$$

The saddle point equation gives:

$$\int_0^\zeta dx' \rho_\zeta(x') \ln |x - x'| = \mu_0 + \mu_1 x. \quad (36)$$

Differentiating with respect to x gives:

$$\mathcal{P} \int_0^\zeta dx' \frac{\rho_\zeta(x')}{x - x'} = \mu_1, \quad (37)$$

where \mathcal{P} denotes the Cauchy principal value. The Tricomi's theorem [60] as explained in Eqs. (18) and (19) is used to invert the above equation along with the constraints $\int_0^\zeta \rho(x) dx = 1$ and $\int_0^\zeta x \rho(x) dx = 1$. Then one obtains the required density as given in Eq. (28). It can be seen that the density in Eq. (28) is valid only for $4/3 \leq \zeta \leq 4$ thus proving the transition point $\zeta = 4/3$. In that case lower boundary L_1 is equal to zero.

The Lagrange multipliers are found as $\mu_0 = \log(\zeta/4) + 4/\zeta - 2$ and $\mu_1 = 4(\zeta - 2)/\zeta^2$. To obtain the saddle point energy first the values of μ_0 and μ_1 are used in Eq. (36) and then using Eq. (33) the energy turns out to be

$$1 - 4 \frac{(\zeta - 1)}{\zeta^2} - \frac{1}{2} \ln \left(\frac{\zeta}{4} \right). \quad (38)$$

In order to calculate the rate function using Eq. (24) one needs to find the saddle point energy when there is no constraint. This is equivalent to putting $\zeta = 4$ in the saddle point energy expression which turns out to be $1/4$. Thus, the rate function using Eq. (24) is given as

$$\Phi(\zeta)_{III} = \frac{3}{4} - 4 \frac{\zeta - 1}{\zeta^2} - \frac{1}{2} \ln \left(\frac{\zeta}{4} \right) \quad (39)$$

and is plotted in Fig. 2 (region **III** of the top figure). This rate function is derived in earlier work Ref.[10] but is given here for the sake of completeness. The second case $1 \leq \zeta \leq 4/3$ is considered in the next subsection.

B. The $1 \leq \zeta \leq \frac{4}{3}$ case

The density of states in Eq. (30) corresponds to the following probability:

$$\begin{aligned} P(N\lambda_{\max} < \zeta) &= P(N\lambda_1 < \zeta, N\lambda_2 < \zeta, \dots, N\lambda_N < \zeta) \\ &= \frac{\int_{L_1}^\zeta \dots \int_{L_1}^\zeta P[\{\lambda_i\}] \prod_{i=1}^N d\lambda_i}{\int_0^\infty \dots \int_0^\infty P[\{\lambda_i\}] \prod_{i=1}^N d\lambda_i}, \end{aligned} \quad (40)$$

when all the eigenvalues are constrained to be smaller than the fixed constant ζ . The lower limit L_1 (whose analytical form is yet to be determined) on the integral in the numerator is chosen based on the numerical simulations for ζ considered in this subsection. Following the similar procedure as used in Sec. III A the effective energy $E_\zeta[\rho]$ is given by

$$\begin{aligned} E_\zeta[\rho] &= -\frac{1}{2} \int_{L_1}^\zeta \int_{L_1}^\zeta dx dx' \rho(x) \rho(x') \ln |x - x'| \\ &+ \mu_0 \left(\int_{L_1}^\zeta dx \rho(x) - 1 \right) + \mu_1 \left(\int_{L_1}^\zeta dx x \rho(x) - 1 \right), \end{aligned} \quad (41)$$

where μ_0 and μ_1 are the Lagrange multipliers enforcing the normalization of the density and the unit trace constraint respectively. For large N , the method of steepest descent gives the same probability as given in Eq. (34) with the effective energy as given in Eq. (41). The saddle point equation which minimizes the effective energy is given as:

$$\int_{L_1}^\zeta dx' \rho_\zeta(x') \ln |x - x'| = \mu_0 + \mu_1 x. \quad (42)$$

Differentiating with respect to x gives:

$$\mathcal{P} \int_{L_1}^\zeta dx' \frac{\rho_\zeta(x')}{x - x'} = \mu_1, \quad (43)$$

where \mathcal{P} denotes the Cauchy principal value. The Tricomi's theorem [60] as explained in Eqs. (18) and (19) is used again to invert the above equation along with the constraints $\int_{L_1}^\zeta \rho(x) dx = 1$ and $\int_{L_1}^\zeta x \rho(x) dx = 1$. Then one obtains the required density given in Eq. (30). It can be seen that the density in Eq. (28) is valid only for $1 \leq \zeta \leq 4/3$ and in that case L_1 turns out to be $4 - 3\zeta$.

The Lagrange multipliers are found as $\mu_0 = 1 + \ln(\zeta - 1) - (3\zeta - 4)/(2(\zeta - 1))$ and $\mu_1 = -1/2(\zeta - 1)$. To obtain the saddle point energy, first the values of μ_0 and μ_1 are used in Eq. (42) and then using Eq. (41) the energy turns out to be $E_\zeta[\rho^*]_\zeta = 1/4 - \ln(\zeta - 1)/2$. It should be noted that this expression is valid only for $1 \leq \zeta \leq 4/3$. In order to calculate the rate function using Eq. (24) one needs to find the saddle point energy when there is no constraint. No constraint on λ_{\max} corresponds to $\zeta = 4$ condition. This energy is calculated using Eq. (38) and turns out to be $1/4$. Thus, the rate function using Eq. (24) is given as $\Phi(\zeta)_{II} = -\ln(\zeta - 1)/2$ and is plotted in Fig. 2 (region **II** of top figure). It can be seen from Eq. (25) that the rate functions $\Phi(\zeta)_I$ and $\Phi(\zeta)_{II}$ are reflection of each other around $\zeta = 1$, in fact it can be seen from the densities in Eqs. (30) and (7) that both are reflection of each other around $\zeta = 1$ provided $2/3 \leq \zeta \leq 1$ is used for the deviations of the minimum eigenvalue. It shows a divergence as $\zeta \rightarrow 1^+$. The rate function $\Phi(\zeta)_{II}$ is derived in earlier work Ref.[10] but is again given here for the sake of completeness. Both the densities given in Eqs. (28) and (30) agrees with each other at $\zeta = 4/3$. In Ref.[10], it is shown that the rate function is continuous and twice differentiable, but its third derivative is discontinuous at $\zeta = 4/3$. Thus, the distribution of eigenvalues shows a third-order phase transition at $\zeta = 4/3$.

At this point it is important to address the earlier works on the distribution of the maximum eigenvalue. In Ref.[10] the rate functions for the large deviations of the maximum eigenvalue are calculated and agrees with ours along with the critical transition at $\zeta = 4/3$. This gives rise to two different regions and the authors has given the nature of optimal densities in these regions. But our analytical calculations (confirmed by numerical simulations) shows that this nature of optimal densities given in [10] is not correct.

The large deviations for the maximum eigenvalue of the Wishart ensemble (where there is no trace constraint) is studied in Ref.[2]. But, no transition in the density as well as the rate function is observed there, which can be attributed to the absence of the trace constraint on the matrices. For the $N = M$ case the density shows divergence at both the ends of its eigenvalue support whenever $\lambda_{\max} < 4$. In this paper it is shown that how the density of states of ρ_A shows the transition as ζ is varied with critical value of $4/3$.

V. BIPARTITE ENTANGLEMENT

In this section, bipartite entanglement between subsystems A and B is studied when there are large deviations in the extreme eigenvalues from their average values. Here, the von Neumann entropy is used as a measure of entanglement [23, 24]. In the earlier works, using the Coulomb gas method the full probability distribution of the Renyi entropy, of which von Neumann entropy is a special case, is derived [7, 10]. There, two critical points are found for which the density shows a transition. In the first transition, the integrable singularity at the origin disappears while in the second, the largest eigenvalue gets detached from the continuum sea of all the other eigenvalues. This transition is different from what is presented in this paper.

As a first case, the large deviations in the case of maximum eigenvalue is considered. As pointed out in the earlier parts of this paper there are two sub cases depending on the position of the barrier. Using Eq. (2) and labeling the eigenvalues of ρ_A by a continuous average density of states as done in Sec. III A the average von Neumann entropy is given as

$$\langle S_{VN} \rangle = -N \int x \ln(x) \rho(x) dx \quad (44)$$

where the form of $\rho(x)$ is given in Eq. (11). One needs to use the appropriate expression of $\rho(x)$ depending on the value of ζ for calculating the entropy. For the case when $4/3 \leq \zeta \leq 4$ the density given in the Eq. (28) is put in Eq. (44). Then using *Mathematica* 9 the average von Neumann entropy is found to be

$$\ln\left(\frac{4N}{\zeta}\right) + \frac{\zeta}{4} - \frac{3}{2}. \quad (45)$$

It is plotted in Fig. 2 for the case $N = 100$ (region **III** of the bottom figure). For the special case of $\zeta = 4$ when there is no constraint on the maximum eigenvalue the average von Neumann entropy equals $\ln(N) - 1/2$ [51]. This value agrees very well with that derived in Ref.[51] where there are no additional constraints on the eigenvalues.

For the second case when $1 \leq \zeta \leq 4/3$ the density given in the Eq. (30) is put in Eq. (44). Again using *Mathematica* 9 the average von Neumann entropy is given

as follows:

$$\begin{aligned} \ln(N) - \frac{1}{\zeta(4-3\zeta)} & \left((\zeta - a)^2 (3\zeta - 4) \times \right. \\ & {}_pF_q \left[\{1, 1, 3/2\}, \{3, 4\}, \frac{4(\zeta - 1)}{3\zeta - 4} \right] + \\ & 2(\zeta - 1)^2 (9\zeta - 10) {}_pF_q \left[\{1, 1, 5/2\}, \{3, 4\}, \frac{4(\zeta - 1)}{3\zeta - 4} \right] \\ & \left. - (3\zeta - 4) (8 - 19\zeta + 11\zeta^2 + \zeta \ln(4 - 3\zeta)) \right) \quad (46) \end{aligned}$$

where ${}_pF_q [a, b, z]$ is the generalized hypergeometric function. It is plotted in Fig. 2 for $N = 100$ (region **II** of the bottom figure). The special case when $\zeta = 1$ is now considered. In that case the maximum eigenvalue is equal to $1/N$. Since there is a trace constraint it can be shown that all the eigenvalues also equals $1/N$. This implies the von Neumann entropy is $\ln(N)$ which is also the maximum value it can take. It can also be evaluated using the Eq. (46). The entropy for $N = 100$ indeed equals $\ln(100) \approx 4.605$. The Eqs. (45) and (46) are compared with the Monte Carlo simulations as shown in Fig. 2. It can be seen that the numerical simulations agrees very well with the analytical results.

Now, the case of the large deviations of the minimum eigenvalue is considered. The barrier position ζ satisfies $0 \leq \zeta \leq 1$. Computing analytical expression for the entropy is difficult. Thus, it is evaluated numerically using the density in Eq. (21) and Eq. (44) for the case of $N = 100$. It is plotted in Fig. 2 (region **I** of the bottom figure) along with the Monte Carlo simulations. It can be seen that both agree with each other very well. Now, the special case when $\zeta = 1$ is considered. In that case the minimum eigenvalue is equal to $1/N$. Due to trace constraint it can be shown that all the eigenvalues are equal to $1/N$. Thus, the von Neumann entropy is $\ln(N)$. It is verified numerically that the entropy agrees with 4.605 for $N = 100$. It can be seen from the plots in regions **I**, **II** and **III** of the bottom figure in Fig. 2 the entropy is continuous and differential function of ζ .

At $\zeta = 4/3$ (the transition between regimes **II** and **III**), the average von Neumann entropy $\langle S_{VN} \rangle$ has a nonanalyticity. It is continuous with $\langle S_{VN} \rangle(4/3) = \ln(3N) - 7/6$ and once differentiable with $\frac{d\langle S_{VN} \rangle}{d\zeta}|_{\zeta=4/3} = -1$. However, the second derivative is discontinuous: $\frac{d^2\langle S_{VN} \rangle}{d\zeta^2}|_{\zeta=4/3^-} = -9/2$ but $\frac{d^2\langle S_{VN} \rangle}{d\zeta^2}|_{\zeta=4/3^+} = 9/16$. Thus, similar to rate function the von Neumann entropy shows a discontinuity but in its second derivative at $\zeta = 4/3$.

VI. ENTANGLEMENT WITHIN SUBSYSTEMS

In this section, the subsystem A is further divided into two parts denoted as 1 and 2 having Hilbert space dimension N_1 and N_2 respectively such that $N = N_1 N_2$. Then

the effect of the large deviations of the extreme eigenvalues of ρ_A are studied on the entanglement between the subsystems 1 and 2. Now, we have a tripartite pure state having dimensions N_1 , N_2 and M . The entanglement in such a tripartite pure system when its state is chosen randomly, has been studied previously [11, 61, 62]. There it is shown that the entanglement between subsystems 1 and 2 shows a transition at $M = 4N_1N_2$ for sufficiently large subsystem dimensions.

The entanglement between subsystems 1 and 2 is studied using the log negativity measure [63]. It is defined as $E_{LN}(\rho_{12}) = \log(\|\rho_{12}^\Gamma\|)$, where $\|\rho^\Gamma\|$ is the trace norm of the partial transpose (PT) matrix ρ^Γ [64]. When the log negativity is greater than zero, the state is said to have the negative partial transpose (NPT). Then in that case the state is entangled. When the log negativity is zero, the state is said to have the positive partial transpose (PPT). Then in that case the state is either separable or bound entangled [65].

Now, the numerical procedure to generate random states ρ_{12} having large deviations in their extreme eigenvalues is given. Every density matrix can be diagonalized by an unitary rotation U . It is thus natural that the distributions of eigenvalues and eigenvectors of ρ_{12} are independent. Thus, the probability measure of ρ_{12} factorizes in a product form [48, 66], $d\mu_x = d\nu_x(\lambda_1, \lambda_2, \dots, \lambda_N) \times dh$. Here, $\lambda_1, \lambda_2, \dots, \lambda_N$ are the eigenvalues of ρ_{12} and the factor dh determines the distribution of its eigenvectors. The probability measure used for the eigenvalues is given in Eq. (3) along with the constraint on the extreme eigenvalues. For the measure dh the unique Haar measure on $U(N)$ is taken which determines the statistical properties of the eigenvectors forming U . Thus, this gives $\rho_{12} = UdU^\dagger$ where d is a diagonal matrix $[\lambda_1, \lambda_2, \dots, \lambda_N]$. The eigenvalues are generated numerically using the Monte Carlo method. Whereas the matrix U is generated using the algorithm given in [67].

Earlier works have studied the effect of PT on ρ_{12} [11, 61, 62]. It is shown that the density of ρ_{12} after PT is very close to the Wigner's semicircle law when the dimensions of both the subsystems are not too small and are of the same order. In these works the extreme eigenvalues fluctuates around their average values. The minimum eigenvalue of ρ_{12}^Γ is shown to follow the Tracy-Widom distribution. Using this the fraction of entangled states at criticality was given. This suggests to investigate the effects of the large deviations of the extreme eigenvalues of ρ_{12} on the density of ρ_{12}^Γ as well as on the entanglement between the subsystems 1 and 2. The results are plotted in Figs. 6, 7 and 8 for the case $N_1 = N_2$. It can be seen that the eigenvalue densities of ρ_{12}^Γ is very close to the Wigner semicircle law. As the barrier position is changed an entanglement transition takes place from dominantly NPT states to dominantly PPT.

It should be mentioned here that the case $N_1 \neq N_2$ without any large deviations in the extreme eigenvalues has been studied in [11]. There it was shown that the den-

sity of states of ρ_{12}^Γ had a skewness which was calculate analytically. It is also observed in our work that the density has a skewness (not presented here) but calculating it analytically seems to be mathematically challenging. Thus, it is not addressed in this paper.

A. Model for shifted semicircles

In the earlier work Ref.[11] the semicircular density of ρ_{12}^Γ was well studied using a simple model. It was suggested by using the fact that the first two moments remains unchanged under the PT operation. The semicircular density depends only on two moments, the mean and the variance. Thus, it was proposed to shift and scale the semicircle of the Gaussian ensembles such that the first two moments of ρ_{12} are matched. To explain the semicircular density obtained in this paper the same model from Ref.[11] is used. The model has been used to accurately predict the transition from the dominantly NPT states to the dominantly PPT states.

Now, the model for the shifted semicircles is given. Here, it is assumed that these random matrices are sampled from the Gaussian unitary ensemble (GUE). Thus, consider

$$Y = X + \frac{I_N}{N} \quad (47)$$

where X is a $N \times N$ random matrix from the GUE ensemble with the necessary matrix element variance such that it matches with that of ρ_{12} , and I_N is the identity matrix of dimension N . It can be seen that $\langle \text{tr}(Y) \rangle = 1$ since $\langle \text{tr}(X) \rangle = 0$, where the angular brackets indicates the ensemble average. Here, the case of large matrix dimension is considered. Thus, it can be expected that the influence of the fact that the $\text{tr}(Y)$ is not exactly equal to one for each and every member of the ensemble will not be observed except in the case of very small dimensional cases.

It can be seen that the eigenvalues of Y are all those of X shifted by $1/N$. Thus, considering the spectrum of X alone will be sufficient. Under the assumption that X is sampled from the GUE it follows that the density of eigenvalues of Y for large N is given as follows:

$$P(\mu) = \frac{2}{\pi R^2} \sqrt{R^2 - \left(\mu - \frac{1}{N}\right)^2}, \quad -R + \frac{1}{N} < \mu < R + \frac{1}{N}, \quad (48)$$

where

$$R = 2\sqrt{\frac{1}{N}\langle \text{tr}(X^2) \rangle} = 2\sqrt{\frac{1}{N}\langle \text{tr}(\rho_{12}^2) \rangle} - \frac{1}{N^2}. \quad (49)$$

Now, the scaled variable $x = \mu N$ is used. This results into the semicircular probability density having a shift of 1 and a rescaled "radius" $\tilde{R} = NR$. Explicitly:

$$P_\Gamma(x) = \frac{2}{\pi \tilde{R}^2} \sqrt{\tilde{R}^2 - (x - 1)^2}, \quad 1 - \tilde{R} < x < 1 + \tilde{R}. \quad (50)$$

This is the the Wigner semicircle law that has been observed in Figs. (6) and (7). Now, \tilde{R} is calculated when there are large deviations in the extreme eigenvalues. This requires to find the average purity of ρ_{12} . First the case of large deviations of the minimum eigenvalue is considered. Using the density of states in Eq. (7) in *Mathematica 9*, the purity turns out to be $\langle \text{tr}(\rho_{12}^2) \rangle = P_1/N = (2 - 2\zeta + \zeta^2)/N$. This gives the rescaled radius $\tilde{R} = 2(1 - \zeta)$ where $0 \leq \zeta \leq 1$. Similarly, for the case of the large deviations of the maximum eigenvalue, the density of states in Eqs. (30) and (28) is used. The purity is found to be $P_1/N = (2 - 2\zeta + \zeta^2)/N$ and $P_3/N = -\zeta(\zeta - 8)/(8N)$ for $1 \leq \zeta \leq 4/3$ and $4/3 \leq \zeta \leq 4$ respectively. Here, P_1 , P_2 and P_3 are the rescaled purities. Using these purities \tilde{R} equals $2(\zeta - 1)$ and $2\sqrt{(-\zeta^2 + 8\zeta - 8)/8}$ for $1 \leq \zeta \leq 4/3$ and $4/3 \leq \zeta \leq 4$ respectively. It can be seen that these analytical expressions for the rescaled radii agrees very well with those from Figs. (6) and (7).

This model gives the NPT-PPT transition very well. It can be seen that the condition for this transition is $\tilde{R} = 1$. Using this condition one obtains $\zeta = 1/2$ and $4 - \sqrt{6}$ as the transition points for the large deviations of the minimum and maximum eigenvalue respectively. For any $\zeta > 1/2$ in the case of minimum eigenvalue and $\zeta < 4 - \sqrt{6}$ in the case of maximum eigenvalue the radius is smaller than one and there are predominantly PPT states. Whereas in the opposite case the lower bound is such that there are predominantly NPT states. Thus, this simple model from Ref.[11] of a shifted random matrix of the GUE kind for the partial transpose gives the transition very well. These critical values of the barrier positions can be observed in Figs. (6) and (7).

In Ref.[11] it was shown analytically that before and after the PT the range of the eigenvalues is the same. Extreme deviations from this result were shown to occur when the state ρ_{12} is pure or nearly pure. For the large deviation of the minimum eigenvalue the density before PT has a support on $[\zeta, 4 - 3\zeta]$ and after PT it becomes $[1 - \tilde{R}, 1 + \tilde{R}]$ where $\tilde{R} = 2(1 - \zeta)$ where $0 \leq \zeta \leq 1$. Thus, the range of the eigenvalues before and after the PT both are equal to $4(1 - \zeta)$.

Similarly, for the large deviations of the maximum eigenvalue the density before PT has a support on $[4 - 3\zeta, \zeta]$ and $[0, \zeta]$ for $1 \leq \zeta \leq 4/3$ and $4/3 \leq \zeta \leq 4$ respectively. After PT the support is again $[1 - \tilde{R}, 1 + \tilde{R}]$ but with $\tilde{R} = 2(1 - \zeta)$ and $2\sqrt{(-\zeta^2 + 8\zeta - 8)/8}$ for $1 \leq \zeta \leq 4/3$ and $4/3 \leq \zeta \leq 4$ respectively. Thus, it can be seen that only for $1 \leq \zeta \leq 4/3$ the range of the eigenvalues before and after PT equals $4(1 - \zeta)$. While for $4/3 \leq \zeta \leq 4$ the range of the eigenvalues after PT is larger than that of before PT except at $\zeta = 4/3$ and 4 where both the ranges are equal. It should be mentioned that these results are valid for the case $N_1 \neq N_2$ since they depend only on $N = N_1 N_2$ and M . But when N_1 and N_2 differ significantly the density of states of ρ_{12}^Γ has a skewness whereas the model predicts zero skewness.

B. Logarithmic negativity

The average log negativity between two subsystems 1 and 2 is now studied. The formalism from Ref.[11] is used again where the fact that the density of states after PT is Wigner's semicircle was used. There it is shown analytically that

$$\langle E_{LN} \rangle_M = \log \left[\frac{2}{\pi} \sin^{-1} \left(\frac{1}{\tilde{R}} \right) + \frac{2}{3\pi\tilde{R}} \sqrt{1 - \frac{1}{\tilde{R}^2}} (1 + 2\tilde{R}^2) \right]. \quad (51)$$

Here, $\langle E_{LN} \rangle_M$ denotes the log negativity obtained using the simple model. For our case, $\tilde{R} = NR = 2(1 - \zeta)$ ($0 \leq \zeta \leq 1$) for the large deviations of the minimum eigenvalue. Whereas, \tilde{R} is $2(\zeta - 1)$ and $2\sqrt{(-\zeta^2 + 8\zeta - 8)/8}$ for $1 \leq \zeta \leq 4/3$ and $4/3 \leq \zeta \leq 4$ respectively for the large deviations of the maximum eigenvalue. This formula is valid only for $\tilde{R} \geq 1$. For the critical case $\tilde{R} = 1$ this formula gives zero for the average log negativity. When $\tilde{R} < 1$, the states obtained are predominantly PPT. In that case $\langle E_{LN} \rangle = 0$. Thus, it can be seen that $\langle E_{LN} \rangle = 0$ for $1/2 \leq \zeta \leq 4 - \sqrt{6}$ since $\tilde{R} \leq 1$ for this range of ζ as shown in the previous subsection. This is plotted in Fig. 8. The Eq. (51) is plotted in Fig. 8 along with numerical results for various values of ζ . It can be seen that Eq. (51) works very well. Consider the situations in which there are no constraints on either of the extreme eigenvalues. It implies $\zeta = 0$ ($\zeta = 4$) for the minimum (maximum) eigenvalue. This gives $\tilde{R} = 2$ for both of them. In that case the Eq. (51) gives $\langle E_{LN} \rangle \approx 0.148702$. This value can be observed in Fig. 8 at $\zeta = 0$ and $\zeta = 4$.

Another interesting features that is observed in Fig. 8 is that there are two different values of ζ 's (ζ_1 and ζ_2 , say) corresponding to the large deviations of the extremes for which entanglement between subsystems 1 and 2 is same. Here, ζ_1 (ζ_2) corresponds to the large deviation of the minimum (maximum) eigenvalue. Thus, this implies $0 \leq \zeta_1 \leq 1$ and $1 \leq \zeta_2 \leq 4$. It can be seen that from Eq. (51) for the log negativity, derived using the simple random matrix model, that two different ζ 's will result in the same log negativity provided \tilde{R} is same for both of them. Whereas in Eq. (49) it is shown that \tilde{R} depends only on the purity of ρ_{12} . Thus, this implies that large deviations of the extremes will have the same log negativity if the corresponding purities (so does the rescaled purities) are same.

Using the simple model it is shown that log negativity is non-zero when $\zeta < 1/2$ ($\zeta > 4 - \sqrt{6}$) for the large deviation of the minimum (maximum) eigenvalue. Thus, it is sufficient to consider the rescaled purities P_1 and P_3 to find the desired relation between ζ_1 and ζ_2 . For given ζ_1 the rescaled purity is $P_1 = 2 - 2\zeta_1 + \zeta_1^2$. The parameter ζ_2 for which the rescaled purity is P_1 one needs to solve for $P_1 = P_3 = (8\zeta_2 - \zeta_2^2)/8$. Solving this quadratic equation one obtains $\zeta_2 = 4 \pm 2\sqrt{2(2 - P_1)} = 4 \pm 2\sqrt{2\zeta_1 - \zeta_1^2}$. Of these two solutions only $\zeta_2 = 4 - 2\sqrt{2(2\zeta_1 - \zeta_1^2)}$ is

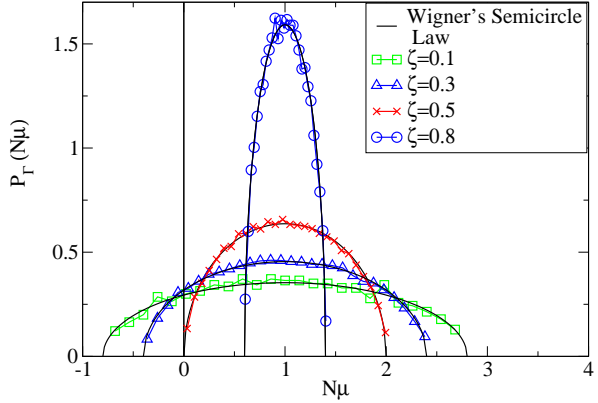


FIG. 6. (Color online) Density of states of ρ_{12}^{Γ} for various values of barrier positions ζ between zero and one. All the eigenvalues of randomly chosen ρ_{12} are greater than the barrier position. One thousand such matrices are used. It corresponds to the large deviations of the minimum eigenvalue ($0 \leq \zeta \leq 1$). A vertical line at the origin has been shown to draw attention to the negative part of the spectrum. Here, $N_1 = N_2 = 10$ and $M = 100$.

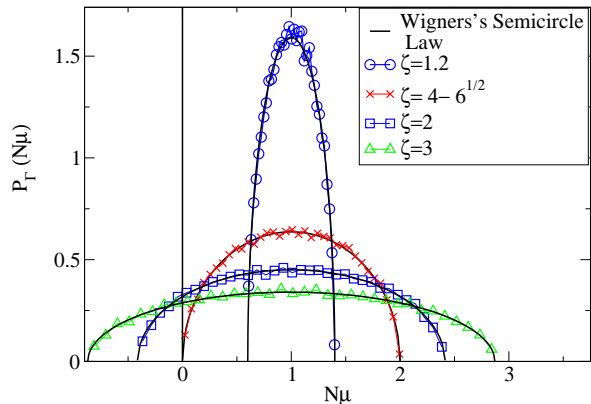


FIG. 7. (Color online) Density of states of ρ_{12}^{Γ} for various values of barrier positions ζ between one and four. All the eigenvalues of randomly chosen ρ_{12} are smaller than the barrier position. One thousand such matrices are used. It corresponds to the large deviations of the maximum eigenvalue ($1 \leq \zeta \leq 4$). A vertical line at the origin has been shown to draw attention to the negative part of the spectrum. Here, $N_1 = N_2 = 10$ and $M = 100$.

valid while the other solution is invalid since it exceeds its upper limit i.e. four. For the special value of $\zeta_1 = 1/8$ the corresponding value of ζ_2 for which the log negativity is same is approximately equal to 2.6307. Using Eq. (51) the log negativity is approximately equal to 0.0919. These results can be observed in Fig. 8. It should be mentioned that these results are valid for the case $N_1 \neq N_2$ since they depend only on $N = N_1 N_2$ and M .

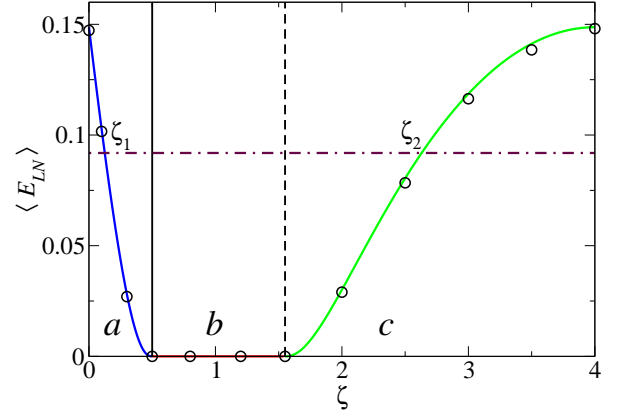


FIG. 8. (Color online) Average entanglement in random states ρ_{12} as measured by the log negativity between subsystems 1 and 2 for various barrier positions. This is compared with the analytical result in Eq. (51) based on the model. Black solid vertical line (dotted line) corresponds to $\zeta = 1/2$ ($\zeta = 4 - 6^{1/2}$) showing the entanglement transition due to large deviations of the minimum (maximum) eigenvalue. Horizontal dash-dotted line is drawn such that ζ (between 0 and 1) corresponding to its intersection with the log negativity is $1/8$. Regions a , b and c corresponds to $0 \leq \zeta \leq 1/2$, $1/2 \leq \zeta \leq 4 - 6^{1/2}$ and $4 - 6^{1/2} \leq \zeta \leq 4$ respectively. Here, $N_1 = N_2 = 10$ and $M = 100$.

VII. SUMMARY AND CONCLUSIONS

This paper has studied the large deviations of the extreme Schmidt eigenvalues in a large bipartite system, denoted as A and B . These eigenvalues play an important role in the study of the entanglement between the two subsystems. Using the Coulomb gas method, the large deviation function for the minimum eigenvalue and the associated equilibrium charge density is derived. Although the large deviation function for the maximum eigenvalue is derived earlier in Ref.[10] the analytical expression for the corresponding equilibrium charge density was lacking. In fact, the qualitative nature of the charge density given in Ref.[10] was incorrect. In this paper, these expressions are derived and are found to agree very well with the Monte Carlo simulations. It is found that, due the large deviations of the maximum eigenvalue the density of states undergoes a transition in which an integrable singularity at the origin disappears. Thus, with these densities generalization of the Marcenko-Pastur function is given when there are large deviations in either of the extreme Schmidt eigenvalues.

The effect of these large deviations is studied on the entanglement between A and B , measured using the von Neumann entropy. In the case of large deviations of the maximum eigenvalue analytical expression for the entropy is derived using *Mathematica 9*, while the same for the minimum eigenvalue remains an open question. The entropy in the later case is obtained by numerical integration. These entropies are found to agree with the

Monte Carlo simulations. The entropy corresponding to the large deviations of the maximum eigenvalue is continuous and once differential, but the second derivative is discontinuous at $\zeta = 4/3$, thus reflecting the transition in the density of states.

One of the subsystem is further divided into two parts, denoted as 1 and 2. The effect of the large deviations is also studied on the entanglement, measured using the log negativity, between 1 and 2. It is found that the state of the subsystem undergoes a NPT-PPT transition. The transition takes place at $\zeta = 0.5$ ($\zeta = 4 - \sqrt{6}$) for the large deviations of the minimum (maximum) eigenvalue. To be precise, when $\zeta > 1/2$ ($\zeta < 4 - \sqrt{6}$) for the large deviations of the minimum (maximum) eigenvalue the states are dominantly PPT, the critical barrier position being $\zeta = 1/2$ ($\zeta = 4 - \sqrt{6}$).

It is found numerically that the density of states of the reduced density matrix of subsystems after PT is close to the Wigner semicircle law when there are large deviations in the extreme Schmidt eigenvalues. The skewness of the semicircle is minimum for the symmetric case $N_1 = N_2$. Earlier work Ref.[11] has shown the same when there are

no such large deviations. Thus, our work shows the robustness of the Wigner semicircle law after PT of ρ_{12} even with the large deviations of its extreme eigenvalues. A simple random matrix model from the same work in Ref.[11] is used successfully to capture the NPT-PPT transition as well as the density of states after PT. One to one relationship between barrier positions ζ_1 and ζ_2 , which corresponds to large deviations of minimum and maximum eigenvalues, is found such that the entanglement between subsystems 1 and 2 is same.

VIII. ACKNOWLEDGMENTS

Author is very grateful to acknowledge many discussions with Arul Lakshminarayan and Karol Życzkowski. Author is happy to acknowledge many discussions with M. S. Santhanam and T. S. Mahesh. Author acknowledges funding from the National Post Doctoral Fellowship (NPDF) of DST-SERB, India, file no. PDF/2015/00050.

[1] F. D. Hollander, *Large Deviations* (American Mathematical Society, 2000)

[2] P. Vivo, S. N. Majumdar, and O. Bohigas, *J. Phys. A: Math. Theor.* **40**, 4317 (2007)

[3] D. S. Dean and S. N. Majumdar, *Phys. Rev. Lett.* **97**, 160201 (2006)

[4] D. S. Dean and S. N. Majumdar, *Phys. Rev. E* **77**, 041108 (2008)

[5] F. L. Metz and I. Pérez Castillo, *Phys. Rev. Lett.* **117**, 104101 (2016)

[6] E. Katzav and I. Pérez Castillo, *Phys. Rev. E* **82**, 040104 (2010)

[7] C. Nadal, S. N. Majumdar, and M. Vergassola, *Phys. Rev. Lett.* **104**, 110501 (2010)

[8] A. Lakshminarayan, S. Tomsovic, O. Bohigas, and S. N. Majumdar, *Phys. Rev. Lett.* **100**, 044103 (2008)

[9] S. N. Majumdar, O. Bohigas, and A. Lakshminarayan, *J. Stat. Phys.* **131**, 33 (2008)

[10] C. Nadal, S. N. Majumdar, and M. Vergassola, *J. Stat. Phys.* **142**, 403 (2011)

[11] U. T. Bhosale, S. Tomsovic, and A. Lakshminarayan, *Phys. Rev. A* **85**, 062331 (2012)

[12] K. Szymański, B. Collins, T. Szarek, and K. Życzkowski, *Journal of Physics A: Mathematical and Theoretical* **50**, 255206 (2017)

[13] M. Chavez, M. Ghil, and J. Urrutia-Fucugauchi, *Extreme Events: Observations, Modeling, and Economics* (Wiley, 2015)

[14] S. Albeverio, V. Jentsch, and H. Kantz, *Extreme Events in Nature and Society* (Springer-Verlag Berlin Heidelberg, 2006)

[15] S. S. Wilks, *Mathematical Statistics* (Princeton University Press, New Jersey, 1947)

[16] K. Fukunaga, *Introduction to Statistical Pattern Recognition* (Elsevier, New York, 1990)

[17] M. Fridman, R. Pugatch, M. Nixon, A. A. Friesem, and N. Davidson, *Phys. Rev. E* **85**, 020101 (2012)

[18] J. G. Richens, J. H. Selby, and S. W. Al-Safi, *Phys. Rev. Lett.* **119**, 080503 (2017)

[19] R. Horodecki, P. Horodecki, M. Horodecki, and K. Horodecki, *Rev. Mod. Phys.* **81**, 865 (2009)

[20] C. H. Bennett, G. Brassard, C. Crépeau, R. Jozsa, A. Peres, and W. K. Wootters, *Phys. Rev. Lett.* **70**, 1895 (1993)

[21] C. H. Bennett and S. J. Wiesner, *Phys. Rev. Lett.* **69**, 2881 (1992)

[22] F. Campaioli, F. A. Pollock, F. C. Binder, L. Céleri, J. Goold, S. Vinjanampathy, and K. Modi, *Phys. Rev. Lett.* **118**, 150601 (2017)

[23] C. H. Bennett, H. J. Bernstein, S. Popescu, and B. Schumacher, *Phys. Rev. A* **53**, 2046 (1996)

[24] I. Bengtsson and K. Zyczkowski, *Geometry of Quantum States: An Introduction to Quantum Entanglement* (Cambridge University Press, Cambridge, 2006)

[25] J. W. Demmel, *Math. Comput.* **50**, 449 (1988)

[26] A. Edelman, *Math. Comput.* **58**, 185 (1992)

[27] M. Znidaric, *J. Phys. A: Math. Theor.* **40**, F105 (2007)

[28] Y. Chen, D.-Z. Liu, and D.-S. Zhou, *J. Phys. A: Math. Theor.* **43**, 315303 (2010)

[29] B. Nadler, *J. Multivariate Anal.* **102**, 363 (2011)

[30] V. A. Marcenko and L. A. Pastur, *Math. USSR-Sb* **1**, 457 (1967)

[31] G. Borot and C. Nadal, *J. Phys. A: Math. Theor.* **45**, 075209 (1997)

[32] B. J-P and P. M, *Theory of Financial Risks* (Cambridge: Cambridge University Press, 2001)

[33] Y. V. Fyodorov and H.-J. Sommers, *J. Math. Phys.* **38**, 1918 (1997)

[34] Y. V. Fyodorov and B. A. Khoruzhenko, *Phys. Rev. Lett.* **83**, 65 (1999)

- [35] E. Shuryak and J. Verbaarschot, Nucl. Phys. A **560**, 306 (1993)
- [36] J. Verbaarschot, Phys. Rev. Lett. **72**, 2531 (1994)
- [37] S. Maslov and Y.-C. Zhang, Phys. Rev. Lett. **87**, 248701 (2001)
- [38] C. Tracy and H. Widom, Commun. Math. Phys. **159**, 151 (1994)
- [39] C. Tracy and H. Widom, Commun. Math. Phys. **177**, 727 (1996)
- [40] S. N. Majumdar and M. Vergassola, Phys. Rev. Lett. **102**, 060601 (2009)
- [41] F. J. Dyson, J. Math. Phys. **3**, 140 (1962)
- [42] F. J. Dyson, J. Math. Phys. **3**, 157 (1962)
- [43] F. J. Dyson, J. Math. Phys. **3**, 166 (1962)
- [44] C. Nadal and S. N. Majumdar, J. Stat. Mech. **2011**, P04001 (2011)
- [45] F. D. Cunden, P. Facchi, and P. Vivo, J. Phys. A: Math. Theor. **49**, 135202 (2016)
- [46] R. Marino, S. N. Majumdar, G. Schehr, and P. Vivo, J. Phys. A: Math. Theor. **47**, 055001 (2014)
- [47] S. Lloyd and H. Pagels, Ann. Phys. **188**, 186 (1988)
- [48] K. Zyczkowski and H.-J. Sommers, J. Phys. A: Math. Gen. **34**, 7111 (2001)
- [49] H.-J. Sommers and K. Zyczkowski, J. Phys. A: Math. Gen. **37**, 8457 (2004)
- [50] E. Lubkin, J. Math. Phys. **19**, 1028 (1978)
- [51] D. Page, Phys. Rev. Lett. **71**, 9 (1993)
- [52] S. Sen, Phys. Rev. Lett. **77**, 1 (1996)
- [53] J. Sanchez-Ruiz, Phys. Rev. E **52**, 5653 (1995)
- [54] P. J. Forrester, *Log-Gases and Random Matrices* (Princeton University Press, Princeton and Oxford, 2010)
- [55] P. Vivo, S. N. Majumdar, and O. Bohigas, Phys. Rev. Lett. **101**, 216809 (2008)
- [56] P. Vivo, S. N. Majumdar, and O. Bohigas, Phys. Rev. B **81**, 104202 (2010)
- [57] A. J. Bray and D. S. Dean, Phys. Rev. Lett. **98**, 150201 (2007)
- [58] S. N. Majumdar, C. Nadal, A. Scardicchio, and P. Vivo, Phys. Rev. Lett. **103**, 220603 (2009)
- [59] S. N. Majumdar, C. Nadal, A. Scardicchio, and P. Vivo, Phys. Rev. E **83**, 041105 (2011)
- [60] F. G. Tricomi, *Integral Equations. Pure Appl. Math., vol. V.* (Interscience, London, 1957)
- [61] G. Aubrun, S. J. Szarek, and D. Ye, Phys. Rev. A **85**, 030302(R) (2012)
- [62] G. Aubrun, S. J. Szarek, and D. Ye, Comm. Pure Appl. Math. **67**, 129 (2014)
- [63] G. Vidal and R. F. Werner, Phys. Rev. A **65**, 032314 (2002)
- [64] A. Peres, Phys. Rev. Lett. **77**, 1413 (1996)
- [65] M. Horodecki, P. Horodecki, and R. Horodecki, Phys. Rev. Lett. **80**, 5239 (1998)
- [66] M. J. Hall, Phys. Lett. A **242**, 123 (1998)
- [67] F. Mezzadri, Notices AMS **54**, 592 (2007)